Improved phase sensitivity in a quantum optical interferometer based on multiphoton catalytic two-mode squeezed vacuum states

Huan Zhang,[1] Wei Ye,[1,2] Chaoping Wei,[3] Ying Xia,[1] Shoukang Chang,[1] Zeyang Liao,[4,*] and Liyun Hu[1,†]

[1]*Center for Quantum Science and Technology, Jiangxi Normal University, Nanchang 330022, China*

[2]*School of Computer Science and Engineering, Central South University, Changsha 410083, China*

[3]*Key Laboratory of Water Information Cooperative Sensing and Intelligent Processing, Nanchang Institute of Technology, Nanchang 330022, China*

[4]*School of Physics, Sun Yat-sen University, Guangzhou 510275, China*

(Received 15 April 2020; revised 11 October 2020; accepted 11 December 2020; published 6 January 2021)

The usage of non-Gaussian states to improve the phase sensitivity of interferometers has been studied before. In this paper, we introduce the multiphoton catalysis two-mode squeezed vacuum (MC-TMSV) state as an input of the Mach-Zehnder interferometer (MZI) and study its phase sensitivity with photon-number parity measurement and the influence of photon losses. We also study the statistical properties of the MC-TMSV state in terms of the average photon number, the Wigner function, and the Mandel-Q parameter. Our results show that the MC-TMSV state can exhibit stronger nonclassical characteristics, thereby making the phase sensitivity more precise with either the increase of the photon-catalyzed number or the decrease of the transmissivity. Furthermore, we also consider the effects of photon losses involving external- and internal-loss processes of the MZI, and we find that in both cases the sensitivity with the MC-TMSV state can be significantly better than that with the TMSV state under the same parameters especially in the serious photon losses and small initial squeezing regimes. We also find that the multiphoton catalysis is more sensitive to the external photon losses compared with the internal ones. Our results here can find important applications in quantum metrology.

DOI: 10.1103/PhysRevA.103.013705

I. INTRODUCTION

The Mach-Zehnder interferometer (MZI) is one of the most important optical interferometers in the field of quantum information, which is usually used to estimate tiny phase changes in quantum metrology [1–10]. How to effectively improve the sensitivity of phase estimation in the MZI has aroused extensive interest in recent years [11–18]. The usual MZI includes three parts (see Fig. 1): the preparation of the input state, the dynamic evolution of interaction with parameters to be measured, and the detection of the output state [19]. The improvement in the precision of phase estimation can be realized from the optimal design of these parts. Many theoretical schemes have been proposed to surpass the standard quantum limit (SQL) $1/\sqrt{N}$ or even reach the Heisenberg limit (HL) $1/N$, in the measurement of a tiny phase shift where N is the average photon number in the input state [20–23]. In addition, the parity measurement of the photon number was proposed in Ref. [15], which shows that the HL can be achieved by maximizing entangled states in a lossless MZI. Caves [20] pointed out that if the nonclassical quantum states, mixing the coherent and squeezed vacuum states, were injected into the MZI, the measurement precision of phase shift could reach the SQL. In order to further increase the phase sensitivity and even reach the HL, many efforts have been dedicated to significantly enhancing the nonclassicality of input quantum states in the MZI systems [24–27]. Thus, how to prepare higher nonclassical quantum states has become an important task, especially for quantum metrology.

Fortunately, the use of non-Gaussian operations to the preparation of input quantum states in the MZI systems has attracted much attention, because it has been proved that higher nonclassical quantum states can be generated by these operations, which may find important applications in quantum precision measurement and quantum information [28–40]. In particular, Anisimov *et al.* have theoretically studied that the application of the two-mode squeezed vacuum (TMSV) state as the input state of an MZI can improve the sensitivity and accuracy of phase measurement and even reach the sub-Heisenberg limit by using the parity detection scheme [40]. However, the maximum two-mode squeezing degree achievable in practice is approximately $r \approx 1.15$, i.e., $\lambda = \tanh r \approx 0.8$ [41], which results in the limited improvement of sensitivity and accuracy of phase measurement. In order to overcome this drawback, Carranza and Gerry proposed a feasible method by using the photon-subtracted TMSV (PS-TMSV) state as input in the MZI systems [42] and showed that the PS-TMSV state can achieve precision better than that of the TMSV state. Based on previous works, Ouyang *et al.* applied the photon-added TMSV (PA-TMSV) state to improve the accuracy of phase shift measurement and found that, for a given initial squeezed degree, the improved precision for the PA-TMSV state is better than that for both the TMSV state and the PS-TMSV state when measuring very

*liaozy7@mail.sysu.edu.cn

†hlyun@jxnu.edu.cn

small phase shifts [43]. Interestingly, except for the photon subtraction and photon addition, quantum catalysis can also be used to effectively improve the nonclassicality of quantum states, while the nonclassical states offer a noticeable improvement in interferometric precision [44–46].

In this paper, we perform a multiphoton catalysis two-mode squeezed vacuum (MC-TMSV state) [47] on the MZI input port and show that the accuracy of phase shift measurement is greatly improved with both the decrease of transitivity and the increase of the catalysis photon number, which is related to the improvement of nonclassicality of the input states. In practical applications, losses and imperfections are avoidable [48–51]. Hence, we also consider the effects of the photon losses placed in front of parity detection (denoted as an external loss) and between the phase shifter and the second beam splitter (BS) (denoted as an internal loss) on the multiphoton catalysis operation. Our results show that in the presence of photon losses the phase sensitivity with multiphoton catalysis can still be better than that with normal squeezed vacuum under the same accessible parameters, particularly in the small initial squeezing regime. We also find that the multiphoton catalysis is more sensitive to the external photon losses in contrast to the internal ones.

This paper is arranged as follows. In Sec. II, we first propose the scheme for generating the MC-TMSV state and then discuss the statistical properties of the generated states in detail. In Sec. III, we mainly focus on the study of the output states of the MZI, which is the evolution of the MC-TMSV state after the MZI, and detect parity signals of one output mode. In Sec. IV, we study quantum Fisher information (QFI) and interference measurement based on parity measurement. In Sec. V, we mainly pay attention to the effects of photon losses in front of the parity detection and between the phase shifter and the second BS on the phase sensitivity. The main results are summarized in Sec. VI.

II. THE STATISTICAL PROPERTIES OF THE MC-TMSV STATE

As shown in Fig. 1(a), we consider the MC-TMSV state as the input of an MZI and mainly study the phase sensitivity of this setup by using the MC-TMSV state (i.e., assuming that the MC-TMSV state has been successfully generated). In principle, the MC-TMSV state can be generated by the schematic setup shown in Fig. 1(b) where an m-photon Fock state $|m\rangle$ is injected into one port of the BS with transmissivity η and simultaneously an ideal photon number resolving detector only registers the same Fock state $|n\rangle$ [47]. This process can be described by an MC operator given by

$$\begin{aligned}\widehat{O}_m &= {}_c\langle m|B(\eta)|m\rangle_c \\ &= G_\eta(b^\dagger b)(\sqrt{\eta})^{b^\dagger b+m},\end{aligned} \tag{1}$$

where $B(\eta) = \exp[(b^\dagger c - bc^\dagger)\arccos\sqrt{\eta}]$ is the BS operator and

$$G_\eta(b^\dagger b) = \frac{\partial^m}{m!\partial\tau^m}\left\{\frac{1}{1-\tau}\left(\frac{1-\tau/\eta}{1-\tau}\right)^{b^\dagger b}\right\}_{\tau=0}, \tag{2}$$

where $\frac{\partial^m}{\partial\tau^m}\{\bullet\}_{\tau=0}$ is a differential operator used to define G. Thus, for our scheme shown in Fig. 1, the proposed MC-TMSV state as the input state of the MZI can be theoretically generated by performing an MC operation on the TMSV, i.e.,

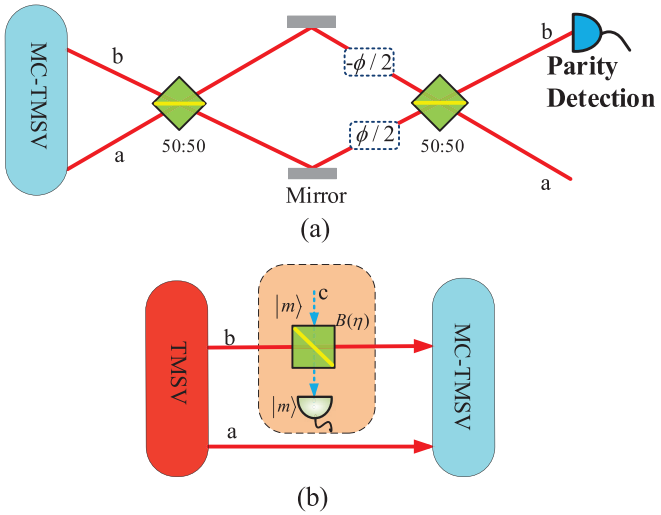

FIG. 1. (a) Schematic diagram of the Mach-Zehnder interferometer for the detection of the phase shift when the multiphoton catalysis two-mode squeezed vacuums are injected into the first beam splitter. (b) Schematic setup for preparing the MC-TMSV state.

$$\begin{aligned}|\text{in}\rangle &= \frac{\widehat{O}_m}{\sqrt{P_m}}S_2(\lambda)|00\rangle \\ &= \frac{W_0}{\sqrt{P_m}}\frac{\partial^m}{\partial\tau^m}\left\{\frac{\exp(a^\dagger b^\dagger W)}{1-\tau}\right\}_{\tau=0}|00\rangle,\end{aligned} \tag{3}$$

where $S_2(\lambda) = \exp\{(a^\dagger b^\dagger - ab)\text{arctanh}\lambda\}$ is a two-mode squeezing operator and P_m represents a normalized coefficient, i.e.,

$$P_m = \frac{\partial^m}{\partial\tau^m\partial\tau_1^m}\epsilon W_0(1-W_1W)_{\tau=\tau_1=0}, \tag{4}$$

with the notations defined as

$$\begin{aligned}W &= \frac{\lambda(\eta-\tau)}{\sqrt{\eta}(1-\tau)}, \\ W_0 &= \frac{\sqrt{\eta^m(1-\lambda^2)}}{m!}, \\ W_1 &= \frac{\lambda(\eta-\tau_1)}{\sqrt{\eta}(1-\tau_1)}, \\ \epsilon &= \frac{1}{(1-\tau)(1-\tau_1)},\end{aligned} \tag{5}$$

where τ and τ_1 are two variables introduced to define W and W_1. It is easily seen from Eq. (3) that the proposed MC-TMSV state $|\text{in}\rangle$ is a non-Gaussian state. Here, we should mention that the preparation of the MC-TMSV state is probabilistic and it is an important factor that need to be considered in practical applications [52]. However, here we mainly focus on the phase sensitivity by using the MC-TMSV state and the effect of success probability will be considered in future research. Actually, the success probability to generate the MC-TMSV states can be very high (the maximum success probability can even approach the unit in the limit of transmissivity

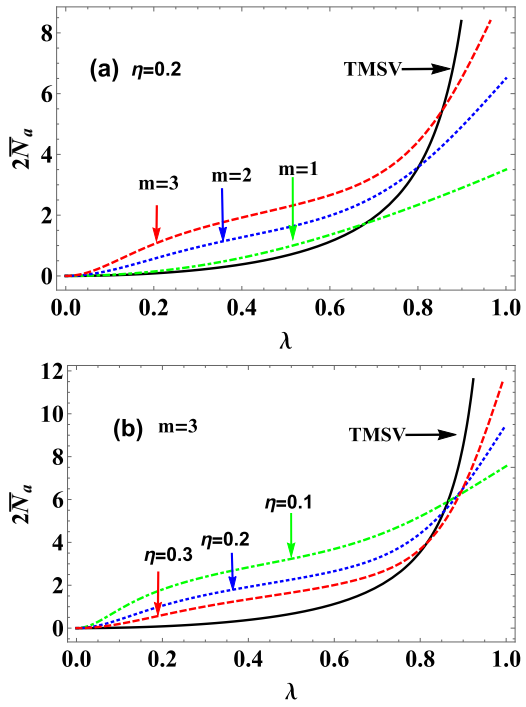

FIG. 2. Average photon number as a function of the squeezing parameter λ for (a) $\eta = 0.2$ and $m = 1$, 2, and 3 and for (b) $m = 3$ and $\eta = 0.1$, 0.2, and 0.3. Solid lines correspond to the TMSV state.

$\eta \to 1$) [47]. However, we should note that, when $\eta = 1$, it returns to the case of usual TMSV states. For the usual MC-TMSV states, the success probability is less than a unit. Interestingly, this quantum state has been used for improving the performances of the entanglement and quantum key distribution [53,54].

In order to better understand the improvement of phase estimation precision, in the following we first discuss the statistical properties of the proposed MC-TMSV state by means of the average photon number, the Wigner function (WF), and the Mandel-Q parameter.

A. Average photon number

Gerry and Mimih have emphasized that the sub-Poissonian statistics is significant for the optical interferometry and the average photon number is an important parameter for evaluating the statistical properties of the light field [15]. For simplicity, according to Eq. (3), here we mainly pay attention to the average photon number of one mode via the relation

$$\overline{N}_a = \langle \mathrm{in}|a^\dagger a|\mathrm{in}\rangle = \widehat{D}\frac{\epsilon}{(1-WW_1)^2} - 1, \tag{6}$$

with

$$\widehat{D} = \frac{W_0^2}{P_m}\frac{\partial^{2m}}{\partial\tau^m\partial\tau_1^m}\{\bullet\}_{\tau=\tau_1=0}. \tag{7}$$

It should be noted that the total average photon number of two modes is $2\overline{N}_a$. Figure 2 shows the average photon number $2\overline{N}_a$ for the proposed state as a function of the squeezing parameter λ for different catalysis photon numbers $m = 1$, 2, and 3 and transmissivity $\eta = 0.1$, 0.2, and 0.3. As a comparison, the black solid line is the average photon number of the TMSV, which is smaller than that of the proposed state in the initial low squeezing λ. In addition, under the same parameters, both the decrease of the transmissivity and the increase of the catalysis photon number for our scheme can increase the average photon number, compared to the TMSV. To be more specific, we can see from Fig. 2(a) that, in the case of low transmissivity $\eta = 0.2$, when given a photon-catalyzed number m, the average photon number for the proposed state is larger than that of the TMSV below a certain threshold λ, e.g., $m = 1$ for $0 < \lambda < 0.68$, and $m = 3$ for $0 < \lambda < 0.86$. Similarly, from Fig. 2(b), at a fixed $m = 3$, we can see that, as the transmissivity decreases, the average photon number can be further increased below a certain threshold λ, e.g., $\eta = 0.1$ for $0 < \lambda < 0.86$, and $\eta = 0.3$ for $0 < \lambda < 0.81$.

B. The Wigner function

The nonclassicality of optical fields can be characterized by the WF in phase space, which provides a good signature for the nonclassicality and the (non-)Gaussianity. In this subsection, let us consider the WF of the input MC-TMSV state in the MZI. The negative volume of the WF represents the existence of the nonclassical characteristics of quantum states [55–57]. According to the definition of the WF, for an arbitrary two-mode state ρ, the corresponding WF in coherent representation is given by

$$W(z,\gamma) = e^{2(|z|^2+|\gamma|^2)}\int\frac{d^2\alpha d^2\beta}{\pi^4}\langle -\alpha,-\beta|\rho|\alpha,\beta\rangle \times \exp[2(z\alpha^* - z^*\alpha) + 2(\gamma\beta^* - \gamma^*\beta)], \tag{8}$$

where $|\alpha,\beta\rangle = |\alpha\rangle\otimes|\beta\rangle$ is the two-mode coherent state. From Eq. (8), evidently, as long as the state ρ is known, one can obtain the analytical expression of the WF. Thus, according to Eq. (3), for our scheme, the input state ρ_{in} can be rewritten as

$$\rho_{\mathrm{in}} = \widehat{D}\epsilon\exp(a^\dagger b^\dagger W)|00\rangle\langle 00|\exp(abW_1). \tag{9}$$

By substituting Eq. (9) into Eq. (8), the WF of the MC-TMSV state can be derived as

$$W(z,\gamma) = \frac{\widehat{D}\epsilon\pi^{-2}}{1-WW_1}e^{\frac{4\gamma zW_1 - 2(W_1W+1)(|z|^2+|\gamma|^2)+4\gamma^*z^*W}{1-WW_1}}. \tag{10}$$

It is obvious that Eq. (10) is a real function and also reveals the non-Gaussian form in phase space. In particular, for the TMSV($\eta = 1$), Eq. (10) reduces to

$$W_0(z,\gamma) = \frac{1}{\pi^2}\exp\left\{-(|z|^2+|\gamma|^2)\frac{2(1+\lambda^2)}{1-\lambda^2} + (z\gamma + z^*\gamma^*)\frac{4\lambda}{1-\lambda^2}\right\}. \tag{11}$$

For the sake of discussion, here we set the squeezing parameter $\lambda = 0.7$, and z and γ are taken as real numbers. Figure 3 shows the WF distribution of the input state ρ_{in} in (z,γ) phase space with different parameters of m and η. Remarkably, for $m = 1$, the negative volume of the WF decreases with the increase of transmissivity $\eta = 0.2$ and 0.4, as shown in Figs. 3(a) and 3(b), respectively. In addition, as can be

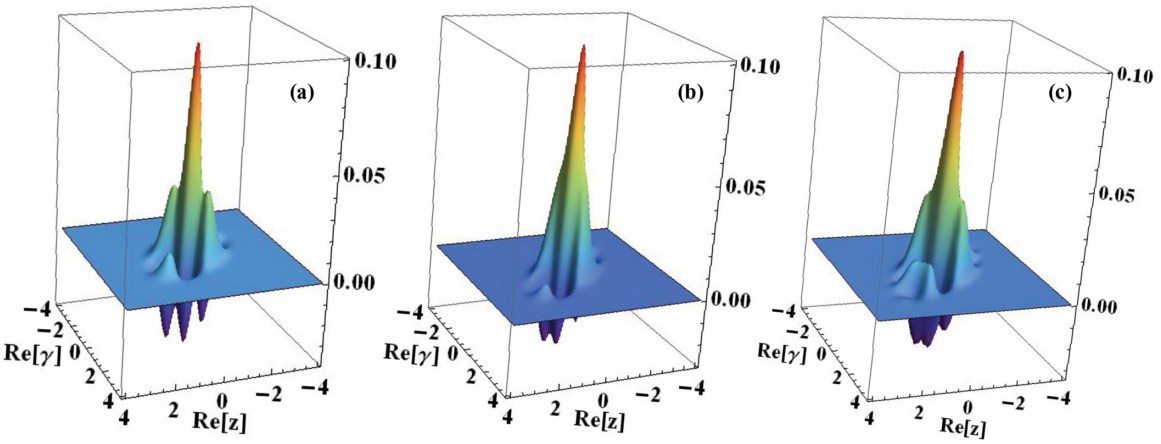

FIG. 3. The Wigner function W of the MC-TMSV state with fixed squeezed parameter $\lambda = 0.7$. (a) $m = 1$ and $\eta = 0.2$, (b) $m = 1$ and $\eta = 0.4$, and (c) $m = 2$ and $\eta = 0.4$.

seen from Figs. 3(b) and 3(c), at fixed $\eta = 0.4$, the negative volume of the WF increases as the catalysis photon numbers $m = 1$ and 2 increase, which means the existence of the higher nonclassicality by increasing m. These results indicate that the nonclassicality of the MC-TMSV state can always appear by modulating the transmissivity and the catalysis photon number.

Furthermore, in order to clearly see the impact of the squeezed parameter on the nonclassicality, we can quantitatively describe nonclassicality of the MC-TMSV state by the value of the negative volume of the WF, which is given by

$$V(z,\gamma) = \frac{1}{2}\left\{\int dx_1 dy_1 dx_2 dy_2 \times[|W(z,\gamma)| - W(z,\gamma)]\right\}. \tag{12}$$

Here, $z = (x_1 + iy_1)/\sqrt{2}$ and $\gamma = (x_2 + iy_2)/\sqrt{2}$. According to Eq. (12), we calculate the negative volume value of the WF for the MC-TMSV state, as shown in Table I. It is worth noting that the maximum two-mode squeezing degree achievable experimentally is about $\lambda \approx 0.8$ [41]. From this practical viewpoint, for simplicity, we only take the squeezed parameter $\lambda \leqslant 0.7$. The negative volume of the WF as a function of the squeezing parameter λ for different m values is shown in Table I. Obviously, in the experimentally achievable squeezing range, the negative volume value of the WF increases with the increase of the squeezed parameter λ for fixed transmissivity $\eta = 0.2$ and $m \in \{1, 2, 3\}$.

TABLE I. Negative volume of the WF.

λ	$m = 1$	$m = 2$	$m = 3$
0	0	0	0
0.1	0.000 439 346	0.004 915 66	0.014 007
0.2	0.009 759 89	0.033 464 3	0.054 410 3
0.3	0.032 176 8	0.064 596 6	0.083 132 1
0.4	0.061 607 3	0.087 958	0.101 32
0.5	0.091 378	0.104 596	0.114 951
0.6	0.116 571	0.115 781	0.127 34
0.7	0.134 41	0.120 984	0.140 167

C. Mandel-Q parameter

The sub-Poisson statistical distribution of the light field is often used as a criterion of the nonclassicality [58,59]. From the distribution of the Mandel-Q parameter, three types of distributions, which correspond to the sub-Poisson, the super-Poisson, and the Poisson, can be identified. Therefore, in this subsection, we mainly analyze the photon statistical distribution of the MC-TMSV state via the Mandel-Q parameter, which is defined as

$$Q = Q_a = Q_b = \frac{\langle a^{\dagger 2}a^2\rangle - \langle a^\dagger a\rangle^2}{\langle a^\dagger a\rangle} = \frac{\langle a^{\dagger 2}a^2\rangle - \overline{N}_a^2}{\overline{N}_a}, \tag{13}$$

where $\overline{N}_a$ has been given in Eq. (6) and the average value $\langle a^{\dagger 2}a^2\rangle$ can be directly calculated as

$$\mathrm{Tr}[a^{\dagger 2}a^2\rho_{\mathrm{in}}] = \widehat{D}\frac{2\epsilon}{(1 - W_1 W)^3} - 3\overline{N}_a + 1. \tag{14}$$

In principle, $Q < 0$ indicates the sub-Poisson distribution, which means the existence of the nonclassicality. In the following, we mainly focus on the condition of $Q < 0$ of the generated state. In Figs. 4(a) and 4(b), we exhibit the Mandel-Q parameter as a function of the squeezing parameter λ and the transmissivity η for several different values of m. As a comparison, the black solid line shows the result of the TMSV. It is easy to see that the light field for the TMSV always presents a super-Poisson distribution ($Q > 1$). For our scheme, at a given transmissivity $\eta = 0.2$, the corresponding Mandel-Q parameter can remain negative in a certain range of λ. In addition, the existing region of the nonclassicality increases with the increase of m [see Fig. 4(a)]. When λ takes a certain value, e.g., $\lambda = 0.6$, the Mandel-Q parameter has a negative value in the small transmissivity range, and this transmissivity range increases as m increases [see Fig. 4(b)], which indicates that the multiphoton catalysis operation is

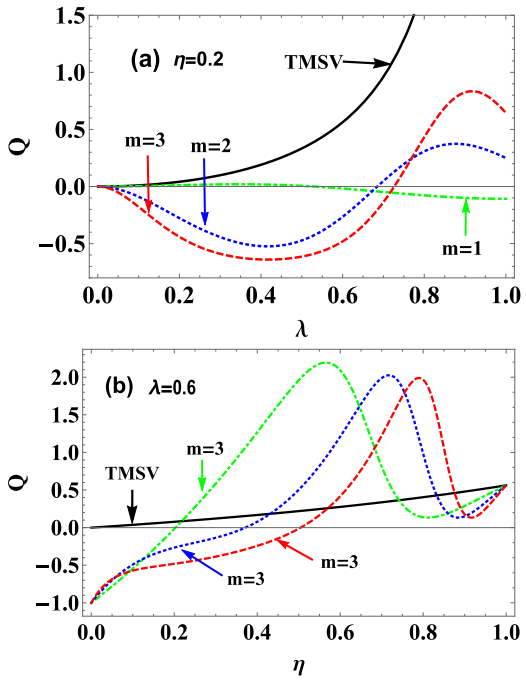

FIG. 4. Plot of the Mandel Q-parameter of the MC-TMSV state. (a) For a given transmissivity $\eta = 0.2$, Mandel Q-parameter as a function of the squeezed parameter λ for different values of $m = 1, 2$, and 3. (b) Mandel-Q parameter as function of transmissivity η with a fixed $\lambda = 0.6$ for different values of $m = 1$, 2, and 3. Solid lines correspond to the TMSV state.

able to effectively prepare nonclassical quantum states. All these results show that the negative value of the Mandel-Q parameter can be obtained by changing the catalysis photon number m, the squeezed parameter λ, and the transmissivity η.

III. PHASE ESTIMATION WITH THE MC-TMSV STATE AS INPUTS OF THE MZI VIA PARITY DETECTION

To approach the HL limit, using the twin Fock states as the inputs of the MZI has been proposed by Holland and Burnett [22], and the parity detection on one output mode proposed by Gerry has been proven to be a viable scheme [28]. In this section, we investigate the phase estimation with the MC-TMSV state injected into a balanced MZI which is composed of two 50:50 BSs and a phase shifter, as depicted in Fig. 1. The behavior of a BS can be characterized as a rotation by applying the renowned Schwinger representation of SU(2) algebra $[J_i, J_j] = i\varepsilon_{ijk}J_k$ $(i, j, k = 1, 2, 3)$, with J_i $(i = 1, 2, 3)$ being an angular momentum operator that can be expressed by two sets of Bose operators [60],

$$J_1 = \tfrac{1}{2}(a^\dagger b + ab^\dagger),\ J_2 = \tfrac{1}{2i}(a^\dagger b - ab^\dagger),$$
$$J_3 = \tfrac{1}{2}(a^\dagger a - b^\dagger b),\ J_0 = \tfrac{1}{2}(a^\dagger a + b^\dagger b), \tag{15}$$

where J_0 represents the Casimir operator that satisfies the commutative relation $[J_0, J_i] = 0$, and both $a(a^\dagger)$ and $b(b^\dagger)$ represent annihilation (creation) operators of two input modes a and b, respectively. Based on the previous work [60], the first BS, the second BS, and the phase shifter can be described by $B_1(\pi/2) = e^{i\frac{\pi}{2}J_1}$, $B_2(-\pi/2) = e^{-i\frac{\pi}{2}J_1}$, and $U(\varphi) = e^{i\varphi J_3}$, respectively. Thus, the unitary transformation associated with such a balanced MZI turns out to be

$$U_{\rm MZ} = e^{-i\frac{\pi}{2}J_1}e^{i\varphi J_3}e^{i\frac{\pi}{2}J_1} = e^{-i\varphi J_2}. \tag{16}$$

In our scheme, according to Eq. (16), the output state of the balanced MZI with the MC-TMSV state input state is given by

$$\begin{aligned}|{\rm out}\rangle &= \exp(-i\varphi J_2)|{\rm in}\rangle_{\rm MZI}\\ &= \widehat{D}'e^{[2Wa^\dagger b^\dagger\cos\varphi + W\sin\varphi(b^{\dagger 2}-a^{\dagger 2})]/2}|00\rangle,\end{aligned} \tag{17}$$

with the notation $\widehat{D}'$ defined as

$$\widehat{D}' = \frac{W_0}{\sqrt{P_m}}\frac{\partial^m}{\partial\tau^m}\frac{1}{1-\tau}\{\bullet\}_{|_{\tau=0}}. \tag{18}$$

Now, let us consider the parity detection placed at one of the output modes in the MZI, as shown in Fig. 1. Generally, the photon-number parity operator in mode b is given by [15,61]

$$\Pi_b = (-1)^{b^\dagger b} = e^{i\pi b^\dagger b}, \tag{19}$$

and its average value is expressed as

$$\langle\Pi_b\rangle = {\rm Tr}[\rho_{\rm out}\Pi_b], \tag{20}$$

where $\rho_{\rm out} = |{\rm out}\rangle\langle{\rm out}|$ can be calculated by Eq. (17). Finally, the average value of the photon-number parity operator can be directly derived as

$$\langle\Pi_b\rangle = \widehat{D}\frac{\epsilon\sqrt{W_2}}{\sqrt{W_3^2 - W_4}}, \tag{21}$$

with

$$\begin{aligned}W_2 &= 1 - WW_1\sin^2\varphi,\\ W_3 &= 1 + WW_1\cos 2\varphi,\\ W_4 &= WW_1[(WW_1 - 1)\sin\varphi]^2,\end{aligned} \tag{22}$$

where $\varphi = \phi + \pi/2$. In particular, when $\eta = 1$, Eq. (21) reduces to

$$\langle\Pi_0\rangle = \frac{1-\lambda^2}{\sqrt{1 - 2\lambda^2\cos 2\phi + \lambda^4}}, \tag{23}$$

which is the TMSV case, as expected [40].

At a fixed squeezing parameter $\lambda = 0.7$, Fig. 5 shows the expectation values of the parity operator $\langle\Pi_b\rangle$ as a function of the phase shift ϕ with different values of η and m. For the TMSV state (black solid line), Anisimov *et al.* [40] noticed that the central peak becomes narrower with the increase of λ, which is interpreted as a form of super-resolution [62]. Obviously, for the case with $m > 0$ and $0 < \eta < 1$, when given a low transmissivity η, the central peak of $\langle\Pi_b\rangle$ at $\phi = 0$ becomes narrower with the increase of $m = 1$, 2, and 3 [see Fig. 5(a)]. In addition, for fixed m, we see that the width of the central peak at $\phi = 0$ decreases significantly with the increase of η]see Fig. 5(b)]. Thus, these results indicate that for the same squeezing parameters λ, the super-resolution enhancement of the MC-TMSV state can be achieved by adjusting the transmissivity η of the BS and the catalysis photon number m.

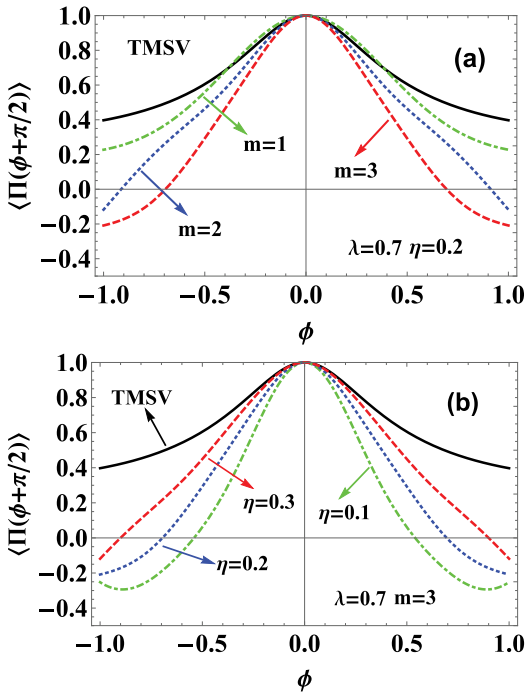

FIG. 5. The expectation value $\langle \Pi_b \rangle$ of the parity operator versus the phase shift ϕ for a given squeezing parameter $\lambda = 0.7$ input state of the MZI. (a) $\eta = 0.3$ and $m = 1$, 2, and 3. (b) $m = 3$ and $\eta = 0.1$, 0.2, and 0.3. Solid lines correspond to the TMSV state.

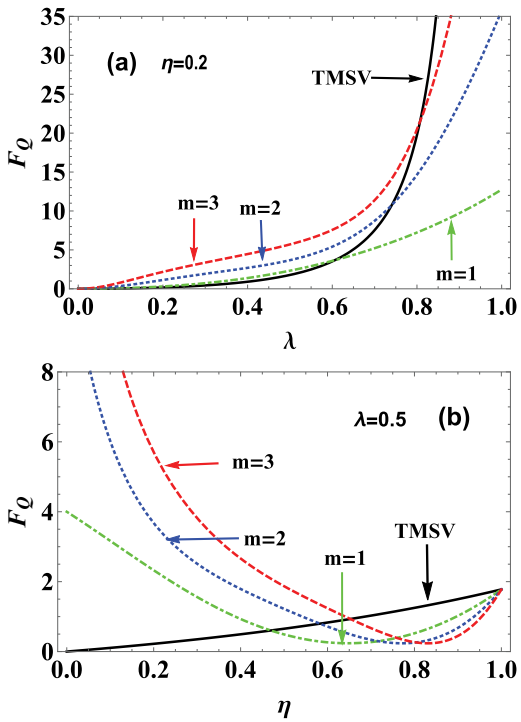

FIG. 6. The quantum Fisher information F_Q as the function of the squeezing parameter λ and the transmissivity η, respectively, for some different catalytic photons m. (a) $\eta = 0.2$. (b) $\lambda = 0.5$. Solid lines correspond to the TMSV state.

IV. QFI AND PHASE UNCERTAINTY

The QFI associated with the well-known quantum Carmer-Rao bound (QCRB) has been widely used to show the phase sensitivity in quantum metrology [63,64]. In addition, according to the QCRB, the lower bound of phase sensitivity is expressed as $\Delta\phi_{\min} = 1/\sqrt{F_Q}$ with the QFI F_Q, which implies that, to achieve the highest sensitivity, the value of F_Q should be maximized. Generally, for an arbitrary pure state injected into the MZI, the F_Q can be calculated as

$$F_Q = 4[\langle \psi' | \psi' \rangle - |\langle \psi' | \psi \rangle|^2], \tag{24}$$

where $|\psi\rangle = e^{i\varphi J_3} e^{i\pi J_1/2} |\text{in}\rangle$ is the state vector after passing through the first BS and the phase shifter of the MZI, and $|\psi'\rangle = \partial|\psi\rangle/\partial\varphi$. Using $|\text{in}\rangle$, Eq. (24) becomes

$$\begin{aligned} F_Q &= 4[\langle \text{in}|J_2^2|\text{in}\rangle - |\langle \text{in}|J_2|\text{in}\rangle|^2] \\ &= -\langle \text{in}|a^{\dagger 2} b^2|\text{in}\rangle - \langle \text{in}|a^2 b^{\dagger 2}|\text{in}\rangle \\ &\quad + 2\overline{N}_a \overline{N}_b + \overline{N}_a + \overline{N}_b, \end{aligned} \tag{25}$$

where $\overline{N}_a$ is given in Eq. (6), and it should be noted that $\overline{N}_b = \overline{N}_a$ in our scheme. Additionally, for our scheme shown in Fig. 1, we can also calculate the expectation value of the general product of operators $a^l b^k a^{\dagger h} b^{\dagger g}$ when the MC-TMSV state is injected into the MZI, i.e.,

$$\begin{aligned} C_{l,k,h,g} &= \text{Tr}[a^l b^k a^{\dagger h} b^{\dagger g} \rho_{\text{in}}] \\ &= \frac{\widehat{D}'' \epsilon}{1 - W W_1} e^{\frac{W_1 t_1 + W s_1 s + s_1 t_1 + s t}{1 - W W_1}}, \end{aligned} \tag{26}$$

with

$$\widehat{D}'' = \frac{\partial^{l+k+h+g}}{\partial s^l \partial s_1^k \partial t^h \partial t_1^g} \{\bullet\}|_{s=s_1=t=t_1=0}. \tag{27}$$

Thus, by combining Eq. (25) with Eq. (26), the explicit form of F_Q for our scheme can be theoretically obtained. To clearly see the behavior of the QFI, in Fig. 6 we show that F_Q as the function of the initial squeezing parameter λ and the transmissivity η. Clearly, we can see from Fig. 6(a) that the QFI becomes larger with the increase of the catalysis photon number ($m = 1$, 2, and 3) in a small range of squeezing parameters when given a transmissivity of $\eta = 0.2$. Dramatically, with the increase of m, the performance of the QFI can be further improved below a certain threshold (e.g., $m = 1$ for $0 < \lambda < 0.60$, $m = 2$ for $0 < \lambda < 0.74$, and $m = 3$ for $0 < \lambda < 0.80$). In addition, from Fig. 6(b), it is clear that, for a given squeezing parameter $\lambda = 0.5$, the QFI of the MC-TMSV state is larger than that of the TMSV when the transmissivity is small, and the width of this region η becomes wider as m increases (e.g., $m = 1$ for $0 < \eta < 0.47$, $m = 2$ for $0 < \eta < 0.58$, and $m = 3$ for $0 < \eta < 0.66$). All these results show that one can obtain a larger QFI by changing the catalysis photon number m and the squeezing parameter λ as well as the transmissivity η. According to the QCRB, these results can be exploited to improve the sensitivity of phase estimation, as expected.

In the above, we have discussed the nonclassicality of MC-TMSV state and the QFI, respectively. Here we study the relation between the nonclassicality of MC-TMSV states and the QFI. In Figs. 7(a) and 7(b), we show the QFI as a function

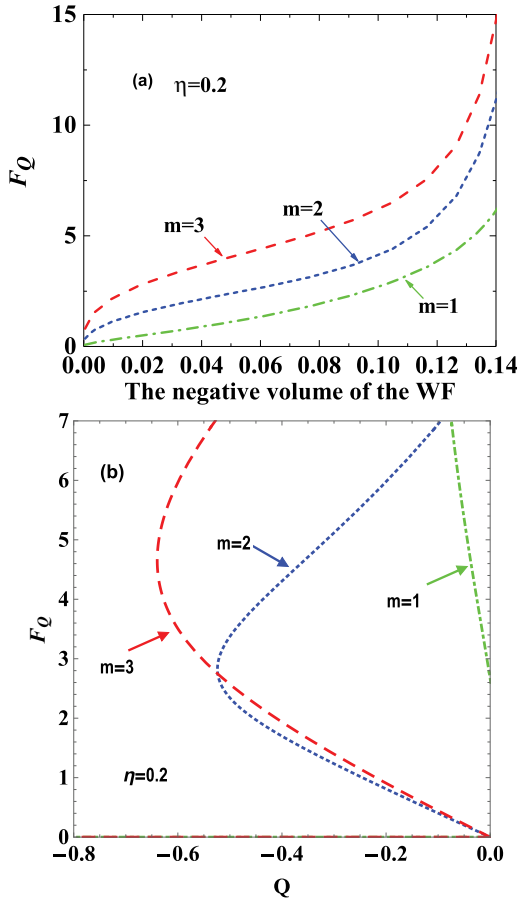

FIG. 7. The QFI as the function of (a) the negative volume of the WF and (b) the Mandel-Q parameter for a given $\eta = 0.2$ and $m = 1$ (green dot-dashed line), $m = 2$ (blue dotted line), and $m = 3$ (red dashed line).

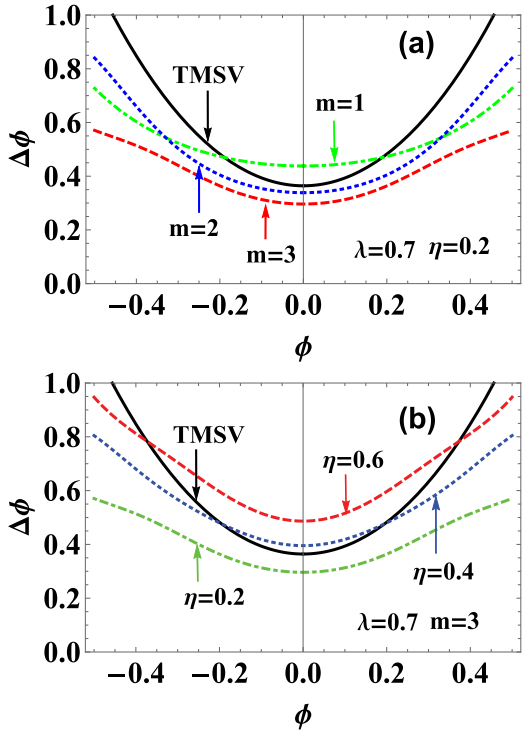

FIG. 8. The phase uncertainty $\Delta\phi$ versus the phase shift ϕ for a given squeezing parameter $\lambda = 0.7$. (a) $\eta = 0.2$ and $m = 1$ and 2. (b) $m = 3$ and $\eta = 0.2$, 0.4, and 0.6. Solid lines correspond to the TMSV state.

of the negative volume of the WF and the Mandel-Q parameter for the input state of the MZI, respectively. Obviously, from Fig. 7(a), we can see that the QFI increases with the increase of the negative volume of the WF for a given $\eta = 0.2$ and $m \in \{1, 2, 3\}$. Furthermore, for a fixed negative volume of the WF, the increase of the catalysis photon number can also lead to the increase of the QFI. From Fig. 7(b), it is seen that the QFI increases when the Mandel-Q parameter becomes smaller when $m = 1$. However, the QFI does not linearly increase with the decrease of the Mandel-Q parameter when $m = 2$ and $m = 3$. This may be due to the fact that the negativity of the Mandel-Q parameter only indicates the existence of nonclassicality but not the magnitude of the nonclassicality.

On the other hand, the phase uncertainty $\Delta\phi$, as an another key signature of optical interferometries, can be determined from the error propagation formula as

$$\Delta\phi = \frac{\Delta\Pi_b}{|\partial\Pi_b/\partial\phi|}, \tag{28}$$

where $\Delta\Pi_b = \sqrt{1 - \langle\Pi_b\rangle^2}$. From Eq. (5), in particular, when $\eta = 1$, Eq. (28) can be simplified to be $\Delta\phi_0 = (1 - 2\lambda^2\cos 2\phi + \lambda^4)/[2\lambda(1 - \lambda^2)\cos\phi]$, which corresponds to the phase uncertainty $\Delta\phi_0$ of the TMSV as inputs [40]. Moreover, the QCRB $\Delta\phi_{\min} = 1/\sqrt{F_Q}$ can be achieved when $\phi \to 0$, which means that the QCRB can be achieved using the parity measurement. To further understand the effects of input state parameters on the phase sensitivity, the phase uncertainty $\Delta\phi$ versus the phase ϕ and the initial squeezing parameter λ are shown in Figs. 8 and 9, respectively.

In Fig. 8(a), we fix the parameters $\lambda = 0.7$ and $\eta = 0.2$ and then plot the $\Delta\phi$ obtained from Eq. (28) as a function of ϕ for $m = 1$, 2, and 3. In all cases, we find that $\Delta\phi$ decreases with the increase of m and even exceeds the TMSV case when $m \geqslant 2$. This means that the multiphoton catalysis operations are beneficial to improving the phase sensitivity. On the other hand, to observe the effect of η on the phase sensitivity, in Fig. 8(b), we illustrate the phase uncertainty as a function of ϕ by setting $\lambda = 0.7$ and $m = 3$ for different transmissivity values of $\eta = 0.2$, 0.4, and 0.6. We can clearly see that the phase uncertainty is reduced with the decrease of the transmissivity, and it can be smaller than that of the TMSV case when $\eta \leqslant 0.2$. In addition, the squeezing parameter λ is another factor that affects the phase sensitivity. Thus, in Fig. 9(a), we plot $\Delta\phi$ as a function of λ for $m = 1$, 2, and 3 for a given $\eta = 0.2$ and $\phi = 0.5$. Obviously, in the range of lower squeezing parameters, $\Delta\phi$ decreases with the increase of m and is lower than that of the TMSV, while for fixed $m = 3$ and $\phi = 0.5$, in Fig. 9(b), it is easy to find that, in the larger region of squeezing parameters, with the increase of η (0.1, 0.2, and 0.3), $\Delta\phi$ decreases and is smaller than that of the TMSV case. In short, we can find a reduction in noise as a result of photon catalytic via adjusting the catalysis photon number m and the squeezing parameter λ as well as the transmissivity η, as expected.

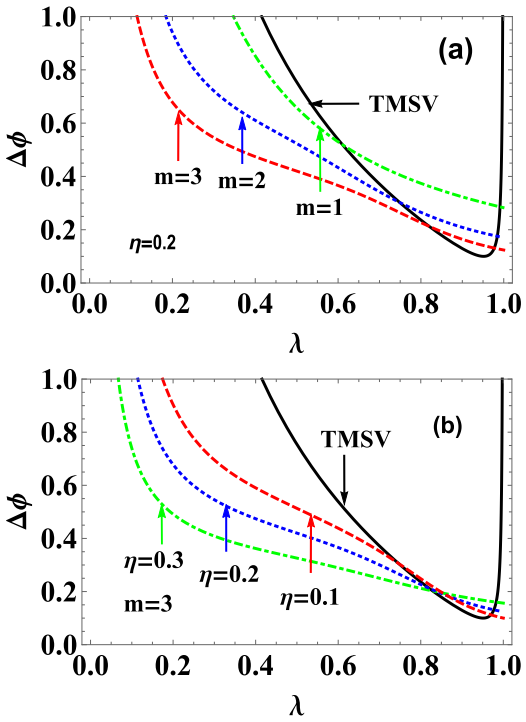

FIG. 9. The phase uncertainty $\Delta\phi$ as a function of the squeezing parameter λ for a given $\phi = 0.5$. (a) $\eta = 0.2$ and $m = 1$, 2, and 3. (b) $m = 3$ and $\eta = 0.1$, 0.2, and 0.3. Solid lines correspond to the TMSV state.

V. EFFECTS OF PHOTON LOSSES ON PHASE SENSITIVITY

In realistic systems, the quantum states are susceptible to the environment, which inevitably affects the phase sensitivity of the MZI. From this point, in this section, we consider the performance of phase sensitivity for our scheme in the presence of photon losses. For the sake of discussion, we assume that the dissipation occurs either in front of the parity detection or between the phase shifter and the second BS, which are shown in Fig. 9.

A. Effects of photon losses in front of parity detection

In this subsection, we first investigate the effects of photon losses in front of the parity detection on the phase sensitivity. As illustrated in Fig. 10(a), the photon-losses process can be simulated by the BS (denoted as B_{κ_1}) with a dissipation factor,

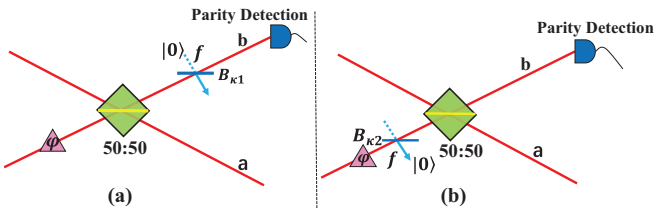

FIG. 10. Schematic diagram of the photon losses is introduced (a) in front of the parity detection and (b) between the phase shifter and the second BS.

κ_1, whose transform relation is

$$B_{\kappa_1}^{\dagger}\begin{pmatrix} b \\ b_f \end{pmatrix} B_{\kappa_1} = \begin{pmatrix} \sqrt{\kappa_1} & \sqrt{1-\kappa_1} \\ -\sqrt{1-\kappa_1} & \sqrt{\kappa_1} \end{pmatrix}\begin{pmatrix} b \\ b_f \end{pmatrix}, \tag{29}$$

where $b_{f1}(b_{f1}^{\dagger})$ are the photon-subtracted (-added) operators of the auxiliary mode f. It should be noted that the smaller the values of κ_1 are, the more serious the photon losses are. In particular, the condition of $\kappa_1 = 1$ corresponds to the ideal case. Since the parity operator Π_b shown in Eq. (19) is inapplicable in the presence of photon losses, we have to derive the parity operator for the photon-losses process (denoted as $\Pi_b^{\rm loss}$). To this end, we rewrite the parity operator in the Weyl ordering representation as [65]

$$\Pi_b = \frac{\pi}{2}\vdots\delta(b)\delta(b^{\dagger})\vdots, \tag{30}$$

where $\vdots\bullet\vdots$ is the symbol of the Weyl ordering and $\delta(\bullet)$ is the delta function [66,67]. By using Eq. (29) and the Weyl ordering invariance under similarity transformations [68,69], the parity operator with the photon-losses process can be expressed as

$$\Pi_b^{\rm loss} = \frac{\pi}{2}{\rm Tr}[|0\rangle_f\langle 0|\vdots\delta(\sqrt{\kappa_1}b + \sqrt{1-\kappa_1}b_f) \times\delta(\sqrt{\kappa_1}b^{\dagger} + \sqrt{1-\kappa_1}b_f^{\dagger})\vdots], \tag{31}$$

where $|0\rangle_f$ denotes the vacuum noise input on the auxiliary mode f. To obtain $\Pi_b^{\rm loss}$, we need to derive the normal ordering form of Eq. (31). While the classical correspondence of any two-mode operator under the Weyl-ordered form $\vdots F(b, b^{\dagger}, b_f, b_f^{\dagger})\vdots$ can be obtained by $b(b^{\dagger})$ being replaced with $\beta(\beta^*)$ and $b_f(b_f^{\dagger})$ being replaced with $\gamma(\gamma^*)$, i.e., $F(b, b^{\dagger}, b_f, b_f^{\dagger})$ becomes $F(\beta, \beta^*, \gamma, \gamma^*)$. Thus, according to the classical correspondence relation of the operator [69]

$$\vdots F(b, b^{\dagger}, b_f, b_f^{\dagger})\vdots = 4\int d^2\beta d^2\gamma F(\beta, \beta^*, \gamma, \gamma^*)\Delta(\beta, \beta^*)\Delta(\gamma, \gamma^*), \tag{32}$$

where $\Delta(\beta, \beta^*) =: \exp[-2(b^{\dagger} - \beta^*)(b - \beta)]:$ and $\Delta(\gamma, \gamma^*) =: \exp[-2(b_f^{\dagger} - \gamma^*)(b_f - \gamma)]:$ are Wigner operators [70,71] and $:\bullet:$ is the symbol of the normal ordering. By substituting Eq. (32) into Eq. (31), for the photon-losses process, the parity operator $\Pi_b^{\rm loss}$ can be calculated as

$$\begin{aligned}\Pi_b^{\rm loss} &= 2\pi\int\frac{d^2\alpha d^2\beta}{\pi^2}\delta(\sqrt{\kappa_1}\beta + \sqrt{1-\kappa_1}\gamma)\delta(\sqrt{\kappa_1}\beta^* \\ &\quad + \sqrt{1-\kappa_1}\gamma^*){\rm Tr}[|0\rangle_f\langle 0|\Delta(\beta, \beta^*)\Delta(\gamma, \gamma^*)] \\ &= :\exp\{-2\kappa_1 b^{\dagger}b\} := (1-2\kappa_1)^{b^{\dagger}b}.\end{aligned} \tag{33}$$

Finally, based on Eq. (17), the average value of $\Pi_b^{\rm loss}$ for the output state can be calculated as

$$\langle\Pi_b^{\rm loss}\rangle = {\rm Tr}[\rho_{\rm out}\Pi_b^{\rm loss}] = \widehat{D}\frac{\epsilon\sqrt{v_1}}{\sqrt{v_2^2 - v_3}}, \tag{34}$$

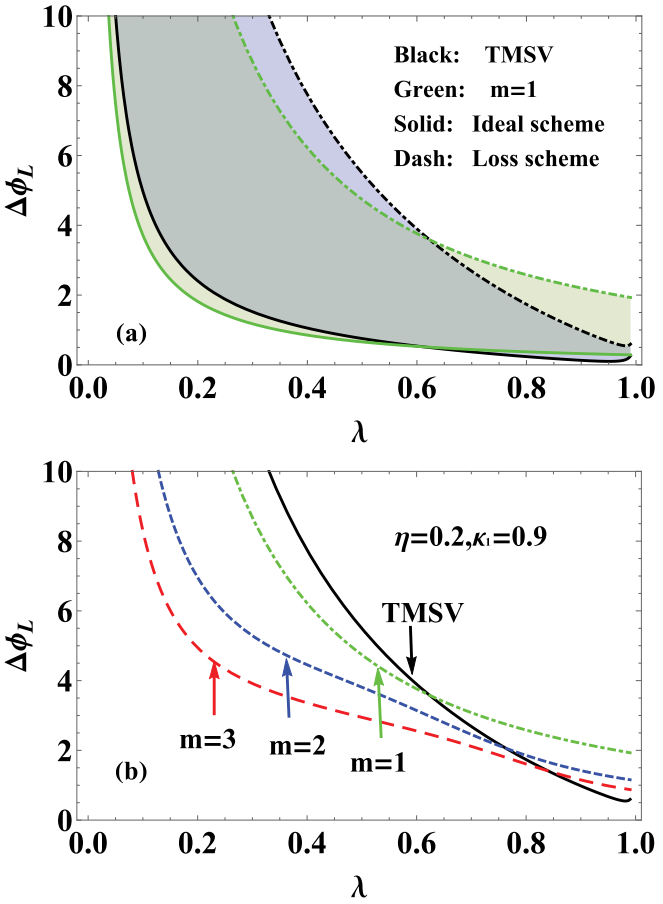

FIG. 11. In the presence of photon losses, the phase uncertainty as a function of the initial squeezed parameters λ at $\phi = 0.05$. (a) Comparison of the ideal case and the loss case for the TMSV and the single-photon catalysis operation. (b) Comparison of the phase uncertainty of the MC-TMSV state with $m = 1$, 2, and 3, and the normal TMSV (black solid line) for 10% photon loss ($\kappa_2 = 0.9$) and $\eta = 0.2$.

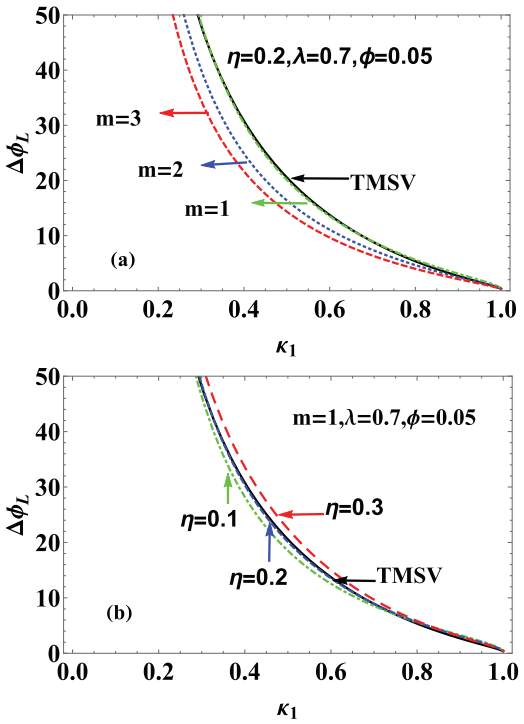

FIG. 12. In the presence of photon losses, the phase uncertainty as a function of the transmissivity of the fictitious beam splitter κ_1 at $\phi = 0.05$ (a) for $\eta = 0.2$, $\lambda = 0.7$, and $m = 1$, 2, and 3 and (b) for $m = 1$, $\lambda = 0.7$, and $\eta = 0.1$, 0.2, and 0.3. Solid lines correspond to the TMSV state.

with

$$\begin{aligned} v_1 &= 1 - WW_1 \sin^2\varphi, \\ v_2 &= W_1 W\left(1 - 2\kappa_1 \cos^2\varphi\right) - 1, \\ v_3 &= (1-2\kappa_1)^2 W_1 W (1 - WW_1)^2 \sin^2\varphi. \end{aligned} \tag{35}$$

Similar to deriving Eq. (28), the phase uncertainty in the presence of photon losses (denoted as $\Delta\phi_L$) is given by

$$\Delta\phi_L = \frac{\Delta\Pi_b^{\text{loss}}}{\left|\partial\Pi_b^{\text{loss}}/\partial\phi\right|}. \tag{36}$$

To clearly see the effects of the different parameters η, m, and λ on the phase uncertainty in the presence of photon losses, we illustrate the phase uncertainty $\Delta\phi_L$ as a function of λ at some fixed parameters, $\kappa_1 = 0.9$ and $\phi = 0.05$, as shown in Fig. 11, from which the photon-losses process has a significant impact on the performance of phase sensitivity. Fortunately, for some given parameters ($\eta = 0.2$, $m = 1$) shown in Fig. 11(a), the phase uncertainty with quantum catalysis, even in the presence of photon losses, still has a better performance in contrast to the TMSV case, particularly in the small-squeezing regime (about $\lambda < 0.6$). Noticeably, compared to the TMSV, the phase uncertainty with multiphoton catalysis under the same dissipation value ($\kappa_1 = 0.9$) can be further improved, but the latter would be worse than the former when λ is greater than a certain threshold value that increases with the increase of m.

On the other hand, to further understand the effects of photon losses on the sensitivity of phase estimation, we also show the phase uncertainty $\Delta\phi_L$ changing with κ_1 at some fixed parameters, $\lambda = 0.7$ and $\phi = 0.05$, as presented in Fig. 12, from which we can find that the phase uncertainty decreases with the decrease of κ_1. For a fixed $m = 1$, it is evident that, in contrast to the TMSV, the phase uncertainty with quantum catalysis can be enhanced in the regime of small κ_1 and low η, which can be seen in Fig. 12(a) (blue dotted and green dot-dashed lines). Based on this point, when given a low transmissivity of $\eta = 0.2$, we can easily find that the phase uncertainty with multiphoton catalysis is superior to that with the TMSV, especially in the small-κ_1 regime. This implies that multiphoton catalysis operations help to resist the photon-losses process in front of parity detection.

B. Effects of photon losses between the phase shifter and the second BS

Next, let us begin with investigating alternative effects of photon losses between the phase shifter and the second BS on the sensitivity of phase estimations, as shown in Fig. 10(b). Likewise, we adopt the BS (denoted as B_{κ_2}) with a dissipation

factor κ_2 to stimulate the photon-losses process. Using the same way described above and after a series of long but direct calculations, the equivalent operator (denoted as $\widetilde{\Pi}_b^{\rm loss}$) of the MZI with photon losses when taking parity detection into account can be given by

$$\begin{aligned}\widetilde{\Pi}_b^{\rm loss} &= {}_f\langle 0|B_1^\dagger U^\dagger(\varphi)B_f^\dagger B_2^\dagger e^{i\pi b^\dagger b}B_2 B_f U(\varphi)B_1|0\rangle_f \\ &= :e^{X_1 a^\dagger a - X_2 b^\dagger a - X_2^* a^\dagger b + X_3 b^\dagger b}:, \end{aligned} \tag{37}$$

where

$$\begin{aligned} X_1 &= \frac{2\sqrt{\kappa_2}\cos\varphi - 1 - \kappa_2}{2}, \\ X_2 &= \frac{(\kappa_2+1)^2 - 4\kappa_2\cos^2\varphi}{4(i\kappa_2 - i + 2\sqrt{\kappa_2}\sin\varphi)}, \\ X_3 &= -\frac{\kappa_2 + 1 + 2\sqrt{\kappa_2}\cos\varphi}{2}, \end{aligned} \tag{38}$$

and we haved used the following transformation relationships [60]:

$$\begin{aligned} B_1^\dagger\begin{pmatrix} a \\ b \end{pmatrix}B_1 &= \frac{\sqrt{2}}{2}\begin{pmatrix} 1 & i \\ i & 1 \end{pmatrix}\begin{pmatrix} a \\ b \end{pmatrix}, \\ B_2^\dagger\begin{pmatrix} a \\ b \end{pmatrix}B_2 &= \frac{\sqrt{2}}{2}\begin{pmatrix} 1 & -i \\ -i & 1 \end{pmatrix}\begin{pmatrix} a \\ b \end{pmatrix}. \end{aligned} \tag{39}$$

Therefore, based on Eq. (37), for a given arbitrary input state $\rho_{\rm in}$, one can easily derive the expectation value of the photon-number parity operator in the presence of photon losses between the phase shifter and the second BS as $\langle\widetilde{\Pi}_b^{\rm loss}\rangle = {\rm Tr}[\rho_{\rm in}\widetilde{\Pi}_b^{\rm loss}]$. Thus, for our scheme, when inputting the MC-TMSV state shown in Eq. (3), it is straightforward to obtain

$$\langle\widetilde{\Pi}_b^{\rm loss}\rangle = {\rm Re}[(1-A_1)^2 - A_2]^{-\frac{1}{2}}, \tag{40}$$

with

$$\begin{aligned} A_1 &= W_1 W(X_1X_3 - \kappa_2 + |X_2|^2), \\ A_2 &= 4|X_2|^2 W_1^2 W^2(X_1X_3 - \kappa_2). \end{aligned} \tag{41}$$

Combining with Eqs. (37) and (40), the phase uncertainty $\Delta\phi_L$ with photon losses in the interior of the MZI can easily be obtained in principle. Similarly, in Fig. 13, we also present the phase uncertainty $\Delta\phi_L$ changing with λ at fixed $\kappa_2 = 0.9$ and $\phi = 0.05$. It is found that the behaviors of these curves are almost consistent with the previous results shown in Fig. 11, which means that, under the same parameters $\kappa_2 = 0.9$ and $\phi = 0.05$, the effects of the above two dissipation models on the accuracy of quantum metrology are almost the same. Further, to show the effects of photon losses inside the MZI on the sensitivity of phase estimation, Fig. 14 illustrates the phase uncertainty $\Delta\phi_L$ as a function of κ_2 at some fixed parameters, $\lambda = 0.7$ and $\phi = 0.05$, from which we can find that, for a given small κ_2, the values of $\Delta\phi_L$ decrease rapidly with the decrease of η and become small with the increase of m. These phenomena are analogous to the case of photon losses in front of parity detection (see Fig. 12).

In order to compare the influence of two kinds of dissipation models on the phase sensitivity, in Fig. 15, at fixed

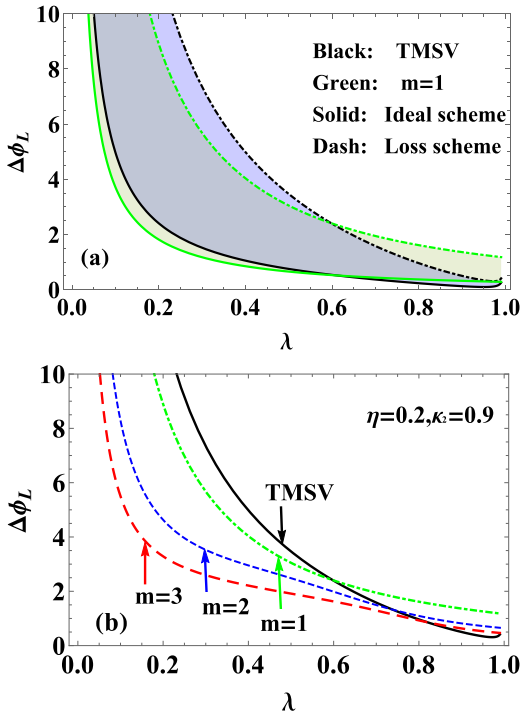

FIG. 13. For photon losses in the interior of the MZI, the phase uncertainty as a function of the initial squeezing parameters λ at $\phi = 0.05$. (a) Comparison of the ideal case and the loss case for the TMSV and the single-photon catalysis operation. (b) Comparison of the phase uncertainty of the MC-TMSV state with $m = 1$, 2, and 3 and the normal TMSV (black solid line) for 10% photon loss ($\kappa_2 = 0.9$) and $\eta = 0.2$.

$\eta = 0.2$, $\lambda = 0.7$, and $\phi = 0.05$, we give the phase uncertainty $\Delta\phi_L$ as a function of $\kappa_1(\kappa_2)$ for several different values of $m = 1$, 2, and 3. It is obvious that the effects of the photon losses in front of parity detection (denoted as external losses) on phase uncertainty are more serious than the case of photon losses in the interior of the MZI (denoted as internal losses) particularly in the small-$\kappa_1(\kappa_2)$ regime. To have a better phase sensitivity in practice, the external photon losses should be suppressed.

VI. CONCLUSION

In summary, we have studied the phase estimation of the MZI with the MC-TMSV state as an input state. In terms of the WF function and the Mandel-Q parameter, the nonclassicality of the MC-TMSV state is presented and it becomes stronger with the decrease of η or the increase of m. The enhancement of the nonclassicality for our state can be exploited to improve the phase sensitivity of the MZI.

To further understand the aforementioned point, by using the parity measurement, we consider the sensitivity of phase estimation when the MC-TMSV state is injected as an input state of the MZI. Our analysis shows that, at a fixed parameter λ, the central peak in the expectation value of the parity operator becomes narrower with the increase of the catalysis photon number m and the decrease of the transmissivity η. Attractively, when the squeezing parameter λ is small, the multiphoton catalysis at low transmissivity can have higher

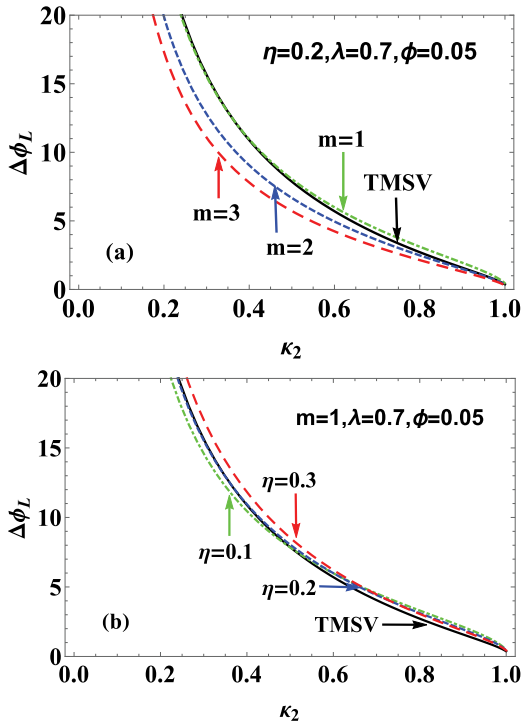

FIG. 14. For photon losses in the interior of the MZI, the phase uncertainty as a function of transmissivity of fictitious beam splitter κ_2 at $\phi = 0.05$ (a) for $\eta = 0.2$, $\lambda = 0.7$ and $m = 1$, 2, and 3, (b) for $m = 1$, $\lambda = 0.7$ and $\eta = 0.1$, 0.2, and 0.3. The black solid lines correspond to the TMSV state.

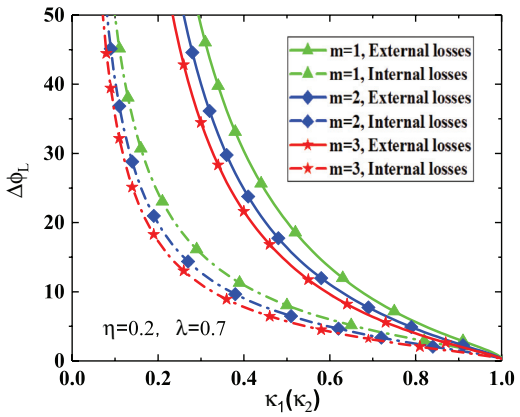

FIG. 15. Comparing the influence of two dissipation ways on the phase sensitivity for $m = 1$ (green), $m = 2$ (blue), $m = 3$ (red) and photon losses in front of the parity detection (solid), in the interior of the MZI (dot-dash).

QFI than that of the TMSV and therefore it can give a more accurate phase sensitivity. Moreover, the QCRB can be reached via the parity measurement with the MC-TMSV state as inputs.

For practical applications, we also study the sensitivity of phase estimation with parity detection in the presence of photon losses. Our results show that, under the same parameters, the sensitivity with the MC-TMSV state in the presence of serious photon losses can be better than that with the normal TMSV, especially in the regimes of the small initial squeezing and low transmissivity. We also find that the external ones have a greater impact on phase sensitivity compared with the internal photon losses, which indicates that multiphoton catalytic states are more robust against the photon loss. Our results here can find important applications in quantum metrology and quantum information.

ACKNOWLEDGMENTS

This work is supported by the National Natural Science Foundation of China (Grants No. 11964013 and No. 11664017) and the Training Program for Academic and Technical Leaders of Major Disciplines in Jiangxi Province. Z.L. is supported by the Key R&D Program of Guangdong Province (Grant No. 2018B030329001) and the Fundamental Research Funds for the Central University (Grant No. 20lgpy163).

[1] J. G. Rarity, P. R. Tapster, E. Jakeman, T. Larchuk, R. A. Campos, M. C. Teich, and B. E. A. Saleh, Two-Photon Interference in a Mach-Zehnder Interferometer, Phys. Rev. Lett. **65**, 1348 (1990).

[2] M. O. Scully and M. S. Zubairy, *Quantum Optics* (Cambridge University, Cambridge, England, 1997).

[3] P. Luca and S. Augusto, Mach-Zehnder Interferometry at the Heisenberg Limit with Coherent and Squeezed-Vacuum Light, Phys. Rev. Lett. **100**, 073601 (2008).

[4] X. Yu, X. Zhao, L. Y. Shen, Y. Y. Shao, J. Liu, and X. G. Wang, Maximal quantum Fisher information for phase estimation without initial parity, Opt. Express **26**, 16292 (2018).

[5] R. Y. Chiao, A. Antaramian, K. M. Ganga, H. Jiao, S. R. Wilkinson, and H. Nathel, Observation of a Topological Phase by Means of a Nonplanar Mach-Zehnder Interferometer, Phys. Rev. Lett. **60**, 1214 (1988).

[6] F. Hudelist, J. Kong, C. J. Liu, J. T. Jing, Z. Y. Ou, and W. P. Zhang, Quantum metrology with parametric amplifier based photon correlation interferometers, Nat. Commun. **5**, 3049 (2014).

[7] T. Nagata, R. Okamoto, J. L. O'Brien, K. Sasaki, and S. Takeuchi, Beating the standard quantum limit with four-entangled photons, Science **316**, 726 (2007).

[8] M. Kacprowicz, R. D. Dobrzan, W. Wasilewski, K. Banaszek, and I. A. Walmsley, Experimental quantum-enhanced estimation of a lossy phase shift, Nat. Photonics **4**, 357 (2010).

[9] K. Goda, O. Miyakawa, E. E. Mikhailov, S. Saraf, R. Adhikari, K. Mckenzie, R. Ward, S. Vass, A. J. Weinstein, and N. Mavalvala, A quantum-enhanced prototype gravitational-wave detector, Nat. Phys. **4**, 472 (2008).

[10] M. G. Genoni, S. Olivares, D. Brivio, S. Cialdi, D. Cipriani, and A. Santamato, Optical interferometry in the presence of large phase diffusion, Phys. Rev. A **85**, 043817 (2012).

[11] L. L. Guo, Y. F. Yu, and Z. M. Zhang, Improving the phase sensitivity of an SU(1,1) interferometer with photon-added squeezed vacuum light, Opt. Express **26**, 29099 (2018).

[12] J. P. Dowling, Quantum optical metrology – the lowdown on high-N00N states, Contemp. Phys. **49**, 125 (2008).

[13] V. Giovannetti, S. Lloyd, and L. Maccone, Advances in quantum metrology, Nat. Photonics **5**, 222 (2011).

[14] M. Schlosshauer, Decoherence, the measurement problem, and interpretations of quantum mechanics, Rev. Mod. Phys. **76**, 1267 (2005).

[15] C. C. Gerry and J. Mimih, The parity operator in quantum optical metrology, Contemp. Phys. **51**, 497 (2010).

[16] S. Pang and A. N. Jordan, Optimal adaptive control for quantum metrology with time-dependent Hamiltonians, Nat. Commun. **8**, 14695 (2017).

[17] W. Ge, K. Jacobs, Z. Eldredge, A. V. Gorshkov, and M. Foss-Feig, Distributed Quantum Metrology with Linear Networks and Separable Inputs, Phys. Rev. Lett. **121**, 043604 (2018).

[18] S. Wang, X. X. Xu, Y. J. Xu, and L. J. Zhang, Quantum interferometry via a coherent state mixed with a photon-added squeezed vacuum state, Opt. Commun. **444**, 102 (2019).

[19] C. W. Helstrom, *Quantum Detection and Estimation Theory* (Academic, New York, 1976).

[20] C. M. Caves, Quantum-mechanical noise in an interferometer, Phys. Rev. D **23**, 1693 (1981).

[21] Z. Y. Ou, Complementarity and Fundamental Limit in Precision Phase Measurement, Phys. Rev. Lett. **77**, 2352 (1996).

[22] M. J. Holland and K. Burnett, Interferometric Detection of Optical Phase Shifts at the Heisenberg Limit, Phys. Rev. Lett. **71**, 1355 (1993).

[23] A. S. Holevo, *Probabilistic and Statistical Aspects of Quantum Theory* (North-Holland, Amsterdam, 1982).

[24] V. Giovannetti, S. Lloyd, and L. Maccone, Quantum-enhanced measurements: Beating the standard quantum limit, Science **306**, 1330 (2004).

[25] D. W. Berry, B. L. Higgins, S. D. Bartlett, M. W. Mitchell, G. J. Pryde, and H. M. Wiseman, How to perform the most accurate possible phase measurements, Phys. Rev. A **80**, 052114 (2009).

[26] Y. B. Aryeh, Phase estimation by photon counting measurements in the output of a linear Mach–Zehnder interferometer, J. Opt. Soc. Am. B **29**, 2754 (2012).

[27] M. J. W. Hall, D. W. Berry, M. Zwierz, and H. M. Wiseman, Universality of the Heisenberg limit for estimates of random phase shifts, Phys. Rev. A **85**, 041802(R) (2012).

[28] C. C. Gerry, Heisenberg-limit interferometry with four-wave mixers operating in a nonlinear regime, Phys. Rev. A **61**, 043811 (2000).

[29] C. C. Gerry and R. A. Campos, Generation of maximally entangled photonic states with a quantum-optical Fredkin gate, Phys. Rev. A **64**, 063814 (2001).

[30] X. X. Xu, F. Jia, L. Y. Hu, Z. L. Duan, Q. Guo, and S. J. Ma, Quantum interference between an arbitrary-photon Fock state and a coherent state, J. Mod. Opt. **59**, 1624 (2012).

[31] L. Y. Hu, X. X. Xu, Z. S. Wang, and X. F. Xu, Photon-subtracted squeezed thermal state: Nonclassicality and decoherence, Phys. Rev. A **82**, 043842 (2010).

[32] M. S. Kim, Recent developments in photon-level operations on travelling light fields, J. Phys. B **41**, 133001 (2008).

[33] G. S. Agarwal and K. Tara, Nonclassical properties of states generated by the excitations on a coherent state, Phys. Rev. A **43**, 492 (1991).

[34] W. Ye, W. D. Zhou, H. L. Zhang, C. J. Liu, J. H. Huang, and L. Y. Hu, Laguerre polynomial excited coherent state: Generation and nonclassical properties, Laser Phys. Lett. **14**, 115201 (2017).

[35] J. Wenger, R. Tualle-Brouri, and P. Grangier, Non-Gaussian Statistics from Individual Pulses of Squeezed Light, Phys. Rev. Lett. **92**, 153601 (2004).

[36] A. Zavatta, S. Viciani, and M. Bellini, Quantum-to-classical transition with single-photon-added coherent states of light, Science **306**, 660 (2004).

[37] L. Y. Hu, C. P. Wei, J. H. Huang, and C. J. Liu, Quantum metrology with Fock and even coherent states: Parity detection approaches to the Heisenberg limit, Opt. Commun. **323**, 68 (2014).

[38] Q. S. Tan, J. Q. Liao, X. G. Wang, and F. Nori, Enhanced interferometry using squeezed thermal states and even or odd states, Phys. Rev. A **89**, 053822 (2014).

[39] P. Liu, P. Wang, W. Yang, G. R. Jin, and C. P. Sun, Fisher information of a squeezed-state interferometer with a finite photon-number resolution, Phys. Rev. A **95**, 023824 (2017).

[40] P. M. Anisimov, G. M. Raterman, A. Chiruvelli, W. N. Plick, S. D. Huver, H. Lee, and J. P. Dowling, Quantum Metrology with Two-Mode Squeezed Vacuum: Parity Detection Beats the Heisenberg Limit, Phys. Rev. Lett. **104**, 103602 (2010).

[41] T. Eberle, V. Hadchen, and R. Schnabel, Stable control of 10 dB two-mode squeezed vacuum states of light, Opt. Express **21**, 11546 (2013).

[42] R. Carranza and C. C. Gerry, Photon-subtracted two-mode squeezed vacuum states and applications to quantum optical interferometry, J. Opt. Soc. Am. B **29**, 2581 (2012).

[43] Y. Ouyang, S. Wang, and L. J. Zhang, Quantum optical interferometry via the photon-added two-mode squeezed vacuum states, J. Opt. Soc. Am. B **33**, 1373 (2016).

[44] R. Birrittella, J. Mimih, and C. C. Gerry, Multiphoton quantum interference at a beam splitter and the approach to Heisenberg-limited interferometry, Phys. Rev. A **86**, 063828 (2012).

[45] D. Braun, P. Jian, O. Pinel, and N. Treps, Precision measurements with photon-subtracted or photon-added Gaussian states, Phys. Rev. A **90**, 013821 (2014).

[46] R. D. Dobrzanski, M. Jarzyna, and J. Kołodynski, Quantum limits in optical interferometry, Prog. Opt. **60**, 345 (2015).

[47] L. Y. Hu, Z. Y. Liao, and M. S. Zubairy, Continuous-variable entanglement via multiphoton catalysis, Phys. Rev. A **95**, 012310 (2017).

[48] S. D. Huver, C. F. Wildfeuer, and J. P. Dowling, Entangled Fock states for robust quantum optical metrology, imaging, and sensing, Phys. Rev. A **78**, 063828 (2008).

[49] R. D. Dobrzanski, U. Dorner, B. J. Smith, J. S. Lundeen, W. Wasilewski, K. Banaszek, and I. A. Walmsley, Quantum phase estimation with lossy interferometers, Phys. Rev. A **80**, 013825 (2009).

[50] T. W. Lee, S. D. Huver, H. Lee, L. Kaplan, S. B. McCracken, C. Min, D. B. Uskov, C. F. Wildfeuer, G. Veronis, and J. P. Dowling, Optimization of quantum interferometric metrological sensors in the presence of photon loss, Phys. Rev. A **80**, 063803 (2009).

[51] D. Li, C. H. Yuan, Y. YAO, W. Jiang, M. Li, and W. P. Zhang, Effects of loss on the phase sensitivity with parity detection in an SU(1, 1) interferometer, J. Opt. Soc. Am. B **35**, 1080 (2018).

[52] J. Combes, C. Ferrie, Z. Jiang, and C. M. Caves, Quantum limits on postselected, probabilistic quantum metrology, Phys. Rev. A **89**, 052117 (2014).

[53] Y. Guo, W. Ye, H. Zhong, and Q. Liao, Continuous-variable quantum key distribution with non-Gaussian quantum catalysis, Phys. Rev. A **99**, 032327 (2019).

[54] W. Ye, H. Zhong, Q. Liao, D. Huang, L. Y. Hu, and Y. Guo, Improvement of self-referenced continuous-variable quantum key distribution with quantum photon catalysis, Opt. Express **27**, 17186 (2019).

[55] A. Zavatta, S. Viciani, and M. Bellini, Tomographic reconstruction of the single-photon Fock state by high-frequency homodyne detection, Phys. Rev. A **70**, 053821 (2004).

[56] R. Filip, Gaussian quantum adaptation of non-Gaussian states for a lossy channel, Phys. Rev. A **87**, 042308 (2013).

[57] A. Zavatta, S. Viciani, and M. Bellini, Single-photon excitation of a coherent state: Catching the elementary step of stimulated light emission, Phys. Rev. A **72**, 023820 (2005).

[58] H. J. Kimble, M. Dagenais, and L. Mandel, Photon Antibunching in Resonance Fluorescence, Phys. Rev. Lett. **39**, 691 (1977).

[59] G. S. Agarwal and K. Tara, Nonclassical character of states exhibiting no squeezing or sub-Poissonian statistics, Phys. Rev. A **46**, 485 (1992).

[60] B. Yurke, S. L. McCall, and J. R. Klauder, SU(2) and SU(1, 1) interferometers, Phys. Rev. A **33**, 4033 (1986).

[61] K. P. Seshadreesan, S. Kim, J. P. Dowling, and H. Lee, Phase estimation at the quantum Cramer-Rao bound via parity detection, Phys. Rev. A **87**, 043833 (2013).

[62] K. J. Resch, K. L. Pregnell, R. Prevedel, A. Gilchrist, G. J. Pryde, J. L. O'Brien, and A. G. White, Time-Reversal and Super-Resolving Phase Measurements, Phys. Rev. Lett. **98**, 223601 (2007).

[63] S. L. Braunstein and C. M. Caves, Statistical Distance and the Geometry of Quantum States, Phys. Rev. Lett. **72**, 3439 (1994).

[64] S. Luo, Wigner-Yanase Skew Information and Uncertainty Relations, Phys. Rev. Lett. **91**, 180403 (2003).

[65] L. Y. Hu and H. Y. Fan, Entangled state for constructing a generalized phase-space representation and its statistical behavior, Phys. Rev. A **80**, 022115 (2009).

[66] H. Y. Fan and L. Y. Hu, Two quantum-mechanical photoncount formulas, Opt. Lett. **33**, 443 (2008).

[67] H. Y. Fan and L. Y. Hu, New n-mode squeezing operator and squeezed states with standard squeezing, Europhys. Lett. **85**, 60001 (2009).

[68] H. Y. Fan, Newton–Leibniz integration for ket-bra operators in quantum mechanics (V)—Deriving normally ordered bivariate-normal-distribution form of density operators and developing their phase space formalism, Ann. Phys. (NY) **323**, 1502 (2008).

[69] H. Weyl, Quantenmechanik und gruppentheorie, Z. Phys. **46**, 1 (1927).

[70] E. P. Wigner, On the quantum correction for thermodynamic equilibrium, Phys. Rev. **40**, 749 (1932).

[71] H. Y. Fan and H. R. Zaidi, Application of IWOP technique to the generalized Weyl correspondence, Phys. Lett. A **124**, 303 (1987).